Eur. Phys. J. A (2016) **52**: 61
DOI 10.1140/epja/i2016-16061-x

THE EUROPEAN PHYSICAL JOURNAL A

Regular Article – Theoretical Physics

Neutrino emissivity in the quark-hadron mixed phase of neutron stars*

William M. Spinella[1,2], Fridolin Weber[2,3,a], Gustavo A. Contrera[4,5,6], and Milva G. Orsaria[4,6]

[1] Computational Science Research Center San Diego State University, 5500 Campanile Drive, San Diego, CA 92182, USA
[2] Department of Physics, San Diego State University, 5500 Campanile Drive, San Diego, CA 92182, USA
[3] Center for Astrophysics and Space Sciences, University of California San Diego, 9500 Gilman Drive, La Jolla, CA 92093, USA
[4] CONICET, Rivadavia 1917, 1033 Buenos Aires, Argentina
[5] IFLP, CONICET - Dpto. de Física, UNLP, La Plata, Argentina
[6] Grupo de Gravitación, Astrofísica y Cosmología, Facultad de Ciencias Astronómicas y Geofísicas, Universidad Nacional de La Plata, Paseo del Bosque S/N (1900), La Plata, Argentina

Received: 24 June 2015 / Revised: 12 January 2016
Published online: 22 March 2016 –
Communicated by D. Blaschke

Abstract. Numerous theoretical studies using various equation of state models have shown that quark matter may exist at the extreme densities in the cores of high-mass neutron stars. It has also been shown that a phase transition from hadronic matter to quark matter would result in an extended mixed phase region that would segregate phases by net charge to minimize the total energy of the phase, leading to the formation of a crystalline lattice. The existence of quark matter in the core of a neutron star may have significant consequences for its thermal evolution, which for thousands of years is facilitated primarily by neutrino emission. In this work we investigate the effect a crystalline quark-hadron mixed phase can have on the neutrino emissivity from the core. To this end we calculate the equation of state using the relativistic mean-field approximation to model hadronic matter and a nonlocal extension of the three-flavor Nambu–Jona-Lasinio model for quark matter. Next we determine the extent of the quark-hadron mixed phase and its crystalline structure using the Glendenning construction, allowing for the formation of spherical blob, rod, and slab rare phase geometries. Finally we calculate the neutrino emissivity due to electron-lattice interactions utilizing the formalism developed for the analogous process in neutron star crusts. We find that the contribution to the neutrino emissivity due to the presence of a crystalline quark-hadron mixed phase is substantial compared to other mechanisms at fairly low temperatures ($\lesssim 10^9$ K) and quark fractions ($\lesssim 30\%$), and that contributions due to lattice vibrations are insignificant compared to static-lattice contributions.

1 Introduction

Seconds after the formation of a neutron star the mean free path of neutrinos grows beyond the star's radius, and neutrinos from the core escape easily cooling the new star rapidly. Neutrino emission continues to be the dominant energy loss mechanism of a neutron star for thousands of years until a temperature of about 10^7 K is reached [1]. It has been shown that the presence of quark matter in the core of a neutron star can have a significant impact on the neutrino emissivity, and suggested that this impact could have an observable effect on the star's thermal evolution [2,3]. In this work we investigate the effect that a mixed phase containing quark matter may have on the neutrino emissivity of a neutron star.

If electric charge neutrality in a neutron star is to be treated globally as proposed by Glendenning [4], then the first order phase transition from hadronic matter to quark matter in the core will result in a mixed phase in which both phases of matter coexist. To minimize the total isospin asymmetry energy the two phases will segregate themselves, resulting in positively charged regions of hadronic matter and negatively charged regions of quark matter, with the rare phase occupying sites on a Coulomb lattice. Further, the competition between the Coulomb and surface energy densities will cause the matter to arrange itself into energy minimizing geometric configurations [3].

The presence of the Coulomb lattice and the nature of the geometric configurations of matter in the quark-hadron mixed phase may have a significant effect on the

* Contribution to the Topical Issue on "Exotic matter in neutron stars" edited by David Blaschke, Jürgen Schaffner-Bielich, Hans-Josef Schulze.

[a] e-mail: fweber@mail.sdsu.edu

neutrino emissivity from the core. More specifically, the presence of electrons in the mixed phase will lead to an additional neutrino emissivity mechanism due to interactions with the lattice. This process is analogous to neutrino-pair bremsstrahlung of electrons in the neutron star crust, where ions exist on a lattice immersed in an electron gas, and for which there exists a large body of work (see, for example, [5–11]). The situation is somewhat more complicated in the quark-hadron mixed phase, but the operative interaction is still the Coulomb interaction. Thus, to estimate the neutrino-pair bremsstrahlung of electrons in the quark-hadron mixed phase we rely heavily on this body of work (particularly [11]).

Neutrino emissivity due to the interaction of electrons with a crystalline quark-hadron mixed phase has been previously studied in this manner by Na *et al.* [12]. In the present work we replace the MIT Bag Model used by [12] to describe quark matter with a three-flavor nonlocal variant of the Nambu–Jona-Lasinio model. Next, we extend the range of possible geometric structures in the mixed phase beyond spherical blobs to include rods and slabs, and calculate the associated static lattice contributions to the neutrino emissivity. Phonon contributions to the emissivity for rod and slab geometries are not considered, though a comparison of the phonon and static lattice contributions for spherical blobs is given and indicates that phonon contributions may not be significant. Finally, the extent of the conversion to quark matter in the core is determined for the chosen parameterizations, and this allows for a targeted comparison between emissivity contributions from standard neutrino emission mechanisms (modified Urca, nucleon-nucleon and quark-quark (NN+QQ) bremsstrahlung) and contributions from electron-lattice interactions. In this work the minimal cooling paradigm is assumed, as the mechanism under investigation is not expected to compete with the direct Urca process, but may serve to enhance the cooling of neutron stars in its absence.

This paper is structured as follows. In sect. 2 we discuss the zero temperature equation of state of a neutron star containing hadronic matter, quark matter, and a quark-hadron mixed phase. The crystalline structure of the mixed phase is described in sect. 3. The neutrino emissivity due to interactions between electrons and the crystalline lattice in the quark-hadron mixed phase is described in sect. 4. Our results, including neutron star properties and neutrino emissivity calculations, are presented in sect. 5. Finally, we present our conclusions in sect. 6.

2 Equation of state

2.1 Neutron star crust

The neutron star outer and inner nuclear crust exists at densities between $10^4\,\mathrm{g\,cm^{-3}} \lesssim \epsilon_{\mathrm{Crust}} \lesssim 10^{14}\,\mathrm{g\,cm^{-3}}$ [13]. Matter in the inner crust consists mostly of nuclei in a Coulomb lattice that is immersed in a gas of electrons and, above neutron drip ($\gtrsim 4{\times}10^{11}\,\mathrm{g\,cm^{-3}}$), free neutrons. In this work we use a combination of the Baym-Pethick-Sutherland and Baym-Bethe-Pethick equations of state for the nuclear crust [14, 15]. Compared to the neutron star core the crust has less affect on the neutron star properties that are to be studied in this work.

2.2 Confined hadronic phase

The hadronic phase of neutron star matter exists at densities above that of the crust and is populated by baryons ($B = \{n, p, \Lambda, \Sigma, \Xi\}$) and leptons ($\lambda = \{e^-, \mu^-\}$). To model the hadronic phase we use the relativistic mean-field approximation (RMF), in which the interactions between baryons are described by the exchange of scalar (σ), vector (ω), and isovector (ρ) mesons [16]. The mean-field Lagrangian is given by [13, 17–21]

$$\begin{aligned}\mathcal{L} = \sum_B \bar{\psi}_B \Big[\gamma_\mu \left(i\partial^\mu - g_{\omega B}\omega^\mu - \frac{1}{2} g_{\rho B} \boldsymbol{\tau}\cdot\boldsymbol{\rho}^\mu \right) \\ - (m_n - g_{\sigma B}\sigma) \Big] \psi_B + \frac{1}{2}(\partial_\mu\sigma\partial^\mu\sigma - m_\sigma^2\sigma^2) \\ - \frac{1}{3} b_\sigma m_n (g_\sigma\sigma)^3 - \frac{1}{4} c_\sigma (g_\sigma\sigma)^4 \\ - \frac{1}{4}\omega_{\mu\nu}\omega^{\mu\nu} + \frac{1}{2} m_\omega^2 \omega_\mu\omega^\mu \\ + \frac{1}{2} m_\rho^2 \boldsymbol{\rho}_\mu\cdot\boldsymbol{\rho}^\mu - \frac{1}{4}\boldsymbol{\rho}_{\mu\nu}\cdot\boldsymbol{\rho}^{\mu\nu} \\ + \sum_\lambda \bar{\psi}_\lambda (i\gamma_\mu\partial^\mu - m_\lambda)\psi_\lambda. \end{aligned} \tag{1}$$

The σ and ω mesons are responsible for nuclear binding while the ρ meson is required to obtain the correct value for the empirical symmetry energy. In contrast to σ and ω mesons, which are isoscalars, the ρ meson is an isovector field that manifests itself in the occurrence of the Pauli matrix $\boldsymbol{\tau}$ ($= (\tau^1, \tau^2, \tau^3)$) in eq. (1). The cubic and quartic σ terms in eq. (1) are necessary (at the relativistic mean-field level) to obtain the empirical incompressibility of nuclear matter [19, 20]. The field tensors $\omega_{\mu\nu}$ and $\boldsymbol{\rho}_{\mu\nu}$ are defined as $\omega_{\mu\nu} = \partial_\mu\omega_\nu - \partial_\nu\omega_\mu$ and $\boldsymbol{\rho}_{\mu\nu} = \partial_\mu\boldsymbol{\rho}_\nu - \partial_\nu\boldsymbol{\rho}_\mu$.

The meson-baryon coupling constants ($g_{\sigma N}$, $g_{\omega N}$, $g_{\rho N}$, b_σ, c_σ) of the Lagrangian are set so that the properties of nuclear matter at saturation density are reproduced for the appropriate parameterization (table 1). In this work we employ the GM1 and NL3 parameterizations as in refs. [22, 23]. To fix the meson-hyperon coupling constants g_{mY} we follow the method presented in ref. [24]. The scalar meson-hyperon coupling constants $g_{\sigma Y}$ are fit to the following hypernuclear potentials at saturation density: $U_\Lambda^{(N)} = -28\,\mathrm{MeV}$, $U_\Sigma^{(N)} = +30\,\mathrm{MeV}$, and $U_\Xi^{(N)} = -18\,\mathrm{MeV}$. The vector meson-hyperon coupling constants $g_{\omega Y}$ are fixed in $SU(3)$ flavor symmetry by the mixing angle θ_v and coupling ratio z taken from the Nijmegen extended-soft-core (ESC08) model [25]. The isovector meson-hyperon coupling constants $g_{\rho Y}$ are given by the usual relations, $g_{\rho\Lambda} = 0$ and $g_{\rho\Sigma} = 2g_{\rho\Xi} = 2g_{\rho N}$.

Table 1. Properties of nuclear matter at saturation density for the NL3 and GM1 parameterizations. Properties include the nuclear saturation density ρ_0, energy per nucleon E/N, compression modulus K, effective nucleon mass m_N^*, and asymmetry energy a_{sy}.

Nuclear saturation properties	GM1	NL3
ρ_0 (fm^{-3})	0.153	0.148
E/N (MeV)	−16.3	−16.3
K (MeV)	300	272
m^*/m_N	0.78	0.60
a_{sy} (MeV)	32.5	37.4

The field equations for the baryon fields follow from eq. (1) as follows [2, 13, 17, 18]:

$$(i\gamma^\mu\partial_\mu - m_B)\,\psi_B = -g_{\sigma B}\sigma\psi_B + g_{\omega B}\gamma^\mu\omega_\mu\psi_B + g_{\rho B}\gamma^\mu\,\boldsymbol{\tau}\cdot\boldsymbol{\rho}_\mu\psi_B. \tag{2}$$

The meson fields in (2) are solutions of the following field equations [2, 13, 17, 18]:

$$\left(\partial^\mu\partial_\mu + m_\sigma^2\right)\sigma = \sum_B g_{\sigma B}\bar\psi_B\psi_B - m_N b_N g_{\sigma N}\left(g_{\sigma N}\sigma\right)^2 - c_N g_{\sigma N}\left(g_{\sigma N}\sigma\right)^3, \tag{3}$$

$$\partial^\mu\omega_{\mu\nu} + m_\omega^2\omega_\nu = \sum_B g_{\omega B}\bar\psi_B\gamma_\nu\psi_B, \tag{4}$$

$$\partial^\mu\boldsymbol{\rho}_{\mu\nu} + m_\rho^2\boldsymbol{\rho}_\nu = \sum_B g_{\rho B}\bar\psi_B\boldsymbol{\tau}\gamma_\nu\psi_B. \tag{5}$$

In the mean-field limit, the meson field equations (3) through (5) are given by [2, 13, 17, 18]

$$m_\sigma^2\sigma = \sum_B g_{\sigma B}\frac{2J_B+1}{2\pi^2}\int_0^{k_B}\frac{m_B^*(\sigma)}{\sqrt{k^2+m_B^{*2}(\sigma)}}k^2\,\mathrm{d}k - bm_n g_\sigma(g_\sigma\sigma)^2 - cg_\sigma(g_\sigma\sigma)^3, \tag{6}$$

$$\omega_0 = \sum_B\frac{g_{\omega B}}{m_\omega^2}\rho_B, \tag{7}$$

$$\rho_{03} = \sum_B\frac{g_{\rho B}}{m_\rho^2}I_{3B}\rho_B, \tag{8}$$

where the effective baryon mass $m_B^*(\sigma) = m_B - g_{\sigma B}\sigma$.

To determine the equation of state we solve a nonlinear system consisting of the meson mean-field equations and the charge conservation conditions (baryonic, electric) given by [13, 17, 18]

$$\rho_b - \sum_B\rho_B = 0, \tag{9}$$

$$\sum_B\rho_B q_B + \sum_\lambda\rho_\lambda q_\lambda = 0, \tag{10}$$

where ρ_b is the total baryonic density and q_B and q_λ are the electric charges of baryons and leptons, respectively. Particles in the hadronic phase are subject to the chemical equilibrium condition,

$$\mu_i = b_i\mu_N - q_i\mu_e, \tag{11}$$

where μ_i is the chemical potential and b_i is the baryon number of particle i. New baryon or lepton states are populated when the right-hand side of eq. (11) is greater than the states' chemical potential. The baryonic and leptonic number densities (ρ_B, ρ_λ) are both given by

$$\rho_i = (2J_i+1)\frac{k_i^3}{6\pi^2}\,. \tag{12}$$

The free parameters of the system are the meson mean fields (σ, ω, ρ), and the neutron and electron fermi momenta (k_n, k_e). Finally, the energy density and pressure of the hadronic phase are given by [13, 17, 18]

$$\epsilon_H = \frac{1}{3}bm_n(g_\sigma\sigma)^3 + \frac{1}{4}c(g_\sigma\sigma)^4 + \frac{1}{2}m_\sigma^2\sigma^2 + \frac{1}{2}m_\omega^2\omega_0^2 + \frac{1}{2}m_\rho^2\rho_{03}^2 + \sum_B\frac{2J_B+1}{2\pi^2}\int_0^{k_B}\sqrt{k^2+m_B^{*2}(\sigma)}k^2\,\mathrm{d}k + \sum_\lambda\frac{1}{\pi^2}\int_0^{k_\lambda}\sqrt{k^2+m_\lambda^2}k^2\,\mathrm{d}k, \tag{13}$$

$$p_H = -\frac{1}{3}bm_n(g_\sigma\sigma)^3 - \frac{1}{4}c(g_\sigma\sigma)^4 - \frac{1}{2}m_\sigma^2\sigma^2 + \frac{1}{2}m_\omega^2\omega_0^2 + \frac{1}{2}m_\rho^2\rho_{03}^2 + \frac{1}{3}\sum_B\frac{2J_B+1}{2\pi^2}\int_0^{k_B}\frac{k^4\,\mathrm{d}k}{\sqrt{k^2+m_B^{*2}(\sigma)}} + \frac{1}{3}\sum_\lambda\frac{1}{\pi^2}\int_0^{k_\lambda}\frac{k^4\,\mathrm{d}k}{\sqrt{k^2+m_\lambda^2}}\,. \tag{14}$$

2.3 Deconfined quark phase

If the dense interior of a neutron star contains deconfined quark matter, it will be made of up (u), down (d), and strange (s) quarks in chemical equilibrium with a small number of electrons and muons. To model the quark phase we use a nonlocal extension of the Nambu–Jona-Lasinio model (n3NJL) as described in refs. [22, 23]. The effective action of this model is given by

$$S_E = \int\mathrm{d}^4x\Big\{\bar\psi(x)(i\partial\!\!\!/ - \hat m)\psi(x) + \frac{1}{2}G_S[(\bar\psi(x)\lambda_a\psi(x))^2 + (\bar\psi(x)i\gamma_5\lambda_a\psi(x))^2] + H\big[\det[\bar\psi(x)(1+\gamma_5)\psi(x)] + \det[\bar\psi(x)(1-\gamma_5)\psi(x)]\big] - G_V[(\bar\psi(x)\gamma^\mu\lambda_a\psi(x))^2 + (\bar\psi(x)i\gamma^\mu\gamma_5\lambda_a\psi(x))^2]\Big\}, \tag{15}$$

where f denotes quark flavor (u, d, s), ψ is a chiral $U(3)$ vector that includes the light quark fields, $\psi \equiv (u, d, s)^T$,

$\hat{m} = \mathrm{diag}(m_u, m_d, m_s)$ is the current quark mass matrix, λ_a with $a = 1, \ldots, 8$ denote the generators of $SU(3)$, and $\lambda_0 = \sqrt{2/3}\,\mathbb{1}_{3\times3}$. The coupling constants G_S and H, the strange quark mass m_s, and the three-momentum ultraviolet cutoff parameter Λ, are all model parameters. Their values are taken from ref. [26], *i.e.*, $m_u = m_d = 5.5\,\mathrm{MeV}$, $m_s = 140.7\,\mathrm{MeV}$, $\Lambda = 602.3\,\mathrm{MeV}$, $G_S\Lambda^2 = 3.67$ and $H\Lambda^5 = -12.36$. The vector coupling constant G_V is treated as a free parameter.

For the mean-field approximation, the thermodynamic potential associated with S_E of eq. (15) is given by

$$\begin{aligned}\Omega^{\mathrm{NL}} =& \\ &-\frac{3}{\pi^3}\sum_{f=u,d,s}\int_0^\infty \mathrm{d}p_0\int_0^\infty \mathrm{d}p \\ &\times\ln\left\{\left[\widehat{\omega}_f^2 + M_f^2(\omega_f^2)\right]\frac{1}{\omega_f^2+m_f^2}\right\} \\ &-\frac{3}{\pi^2}\sum_{f=u,d,s}\int_0^{\sqrt{\mu_f^2-m_f^2}}\mathrm{d}p p^2\left[(\mu_f - E_f)\,\theta\left(\mu_f - m_f\right)\right] \\ &-\frac{1}{2}\left[\sum_{f=u,d,s}\left(\bar{\sigma}_f\bar{S}_f + \frac{G_S}{2}\bar{S}_f^2\right) + \frac{H}{2}\bar{S}_u\,\bar{S}_d\,\bar{S}_s\right] \\ &-\sum_{f=u,d,s}\frac{\overline{\omega}_f^2}{4G_V}\,, \end{aligned} \tag{16}$$

where $\bar{\sigma}_f$, $\overline{\omega}_f$, and $\bar{S}_f$ are the quark scalar, vector, and auxiliary mean fields, respectively. Moreover, we have $E_f = \sqrt{\boldsymbol{p}^2 + m_f^2}$, $\omega_f^2 = (p_0 + i\mu_f)^2 + \boldsymbol{p}^2$, and $M_f(\omega_f^2) = m_f + \bar{\sigma}_f g(\omega_f^2)$ are the momentum-dependent quark masses. The quantity $g(\omega_f^2) = \exp(-\omega_f^2/\Lambda^2)$ is the form factor which introduces nonlocality into the quark interactions [22, 23]. The auxiliary mean fields are given by

$$\bar{S}_f = -48\int_0^\infty \mathrm{d}p_0\int_0^\infty \frac{\mathrm{d}p}{8\pi^3}g(\omega_f^2)\frac{M_f(\omega_f^2)}{\widehat{\omega}^2 + M_f^2(\omega_f^2)}\,. \tag{17}$$

Due to the inclusion of the vector interaction the quark chemical potentials are shifted as follows:

$$\widehat{\mu}_f = \mu_f - g(w_f^2)\overline{\omega}_f, \tag{18}$$

$$\widehat{\omega}_f^2 = (p_0 + i\widehat{\mu}_f)^2 + p^2. \tag{19}$$

The scalar and vector mean fields are obtained by minimizing the grand thermodynamic potential,

$$\frac{\partial\Omega^{\mathrm{NL}}}{\partial\bar{\sigma}_f} = 0, \qquad \frac{\partial\Omega^{\mathrm{NL}}}{\partial\overline{\omega}_f} = 0. \tag{20}$$

The quark number densities are given by

$$\rho_f = \frac{\partial\Omega^{\mathrm{NL}}}{\partial\mu_f}\,. \tag{21}$$

To determine the equation of state, one must solve a nonlinear system of equations for the fields $\bar{\sigma}_f$ and $\bar{\omega}_f$, and the neutron and electron chemical potentials μ_n and μ_e. This system of equations consists of the mean-field equations,

$$\bar{\sigma}_i + G_S\bar{S}_i + \frac{1}{2}H\bar{S}_j\bar{S}_k = 0, \tag{22}$$

with cyclic permutations over the quark flavors,

$$\overline{\omega}_f - 2G_V\frac{\partial\Omega^{\mathrm{NL}}}{\partial\omega_f} = 0, \tag{23}$$

and the charge conservation equations,

$$\sum_{f=u,d,s}\rho_f - 3\rho_b = 0, \tag{24}$$

$$\sum_{f=u,d,s}\rho_f q_f + \sum_{\lambda=e^-,\mu^-}\rho_\lambda q_\lambda = 0. \tag{25}$$

Finally, the pressure and energy density are given by

$$p_Q = \Omega_0 - \Omega^{\mathrm{NL}}, \tag{26}$$

$$\epsilon_Q = -p_Q + \sum_{f=u,d,s}\rho_f\mu_f + \sum_{\lambda=e^-,\mu^-}\rho_\lambda\mu_\lambda, \tag{27}$$

where Ω_0 is the grand thermodynamic potential Ω^{NL} calculated for $\mu_f = \overline{\omega}_f = 0$.

2.4 Quark-hadron mixed phase

When the pressure in the hadronic phase grows to a level equal to that of the quark phase at the same baryonic density a first-order phase transition from hadronic matter to quark matter may begin. Since a theory that can treat both the hadronic and quark phases simultaneously is currently unavailable, we construct the mixed phase by blending RMF and n3NJL. Each phase is solved for separately, and then the two are blended together under the Gibbs condition, $p_H = p_Q$. The pressure (p_M) and energy density (ϵ_M) in the mixed phase are given by [3, 4]

$$p_M = \frac{1}{2}(p_H + p_Q), \tag{28}$$

and

$$\epsilon_M = (1-\chi)\epsilon_H + \chi\epsilon_Q, \tag{29}$$

where $\chi = V_Q/V_{\mathrm{Total}}$ is the quark fraction of the mixed phase. Other properties such as the particle number densities can be handled in a similar fashion.

3 Crystalline structure of the quark-hadron mixed phase

A mixed phase of hadronic and quark matter will arrange itself so as to minimize the total energy of the phase. Under the condition of global charge neutrality this is the same as minimizing the contributions to the total energy due to phase segregation, which includes the surface

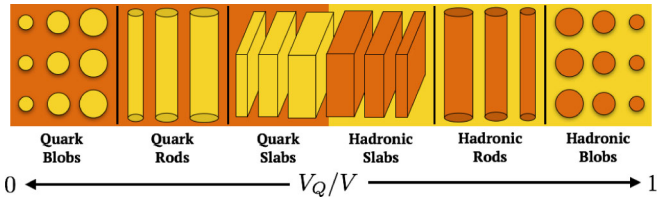

Fig. 1. (Color online) Spherical blob, rod, and slab rare phase structures. $V_Q/V_{\rm Total}$ denotes the quark fraction of the mixed phase.

and Coulomb energy contributions. Expressions for the Coulomb (ϵ_C) and surface (ϵ_S) energy densities can be written as [3]

$$\epsilon_C = 2\pi e^2 \left[q_H(\chi) - q_Q(\chi)\right]^2 r^2 x f_D(x), \quad (30)$$

$$\epsilon_S = Dx\sigma(\chi)/r, \quad (31)$$

where q_H (q_Q) is the hadronic (quark) phase charge density, and r is the radius of the rare phase structure. The quantities x and $f_D(x)$ in eq. (30) are defined as

$$x = \min(\chi, 1-\chi) \quad (32)$$

and

$$f_D(x) = \frac{1}{D+2}\left[\frac{1}{D-2}\left(2 - Dx^{1-2/D}\right) + x\right], \quad (33)$$

where D is the dimensionality of the lattice. The quantity $\sigma(\chi)$ in eq. (31) denotes the surface tension.

The phase rearrangement process will result in the formation of geometrical structures of the rare phase distributed in a crystalline lattice that is immersed in the dominant phase (fig. 1). The rare phase structures are approximated for convenience as spherical blobs, rods, and slabs [3]. The spherical blobs occupy sites in a three-dimensional ($D = 3$) body centered cubic (BCC) lattice, the rods in a two-dimensional ($D = 2$) triangular lattice, and the slabs in a simple one-dimensional ($D = 1$) lattice [11]. At $\chi = 0.5$ both hadronic and quark matter exist as slabs in the same proportion, and at $\chi > 0.5$ the hadronic phase becomes the rare phase with its geometry evolving in reverse order (from slabs to rods to blobs).

3.1 Surface tension of the quark-hadron interface

Direct determination of the surface tension of the quark-hadron interface is problematic because of difficulties in constructing a single theory that can accurately describe both hadronic matter and quark matter. Therefore, we employ an approximation proposed by Gibbs where the surface tension is taken to be proportional to the difference in the energy densities of the interacting phases [3],

$$\sigma(\chi) = \eta L \left[\epsilon_Q(\chi) - \epsilon_H(\chi)\right], \quad (34)$$

where L is proportional to the surface thickness which should be on the order of the strong interaction (1 fm), and

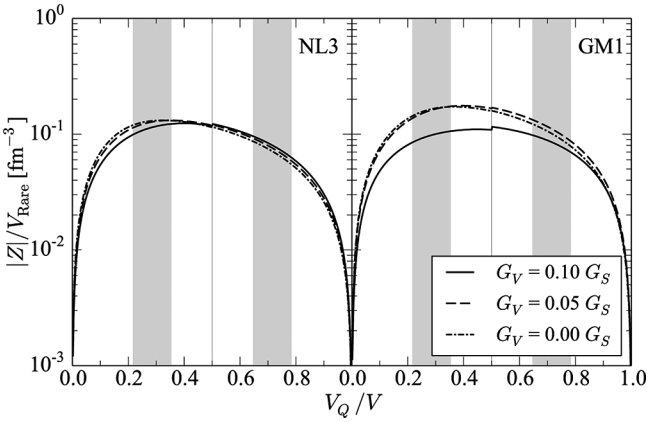

Fig. 2. (Color online) Rare phase structure charge number per unit volume plotted against quark fraction for the given parameterizations and vector coupling constant values. Slight discontinuity at $\chi = 0.5$ is due to a higher number of positively charged baryons (electrons make up difference in negative charge).

η is a proportionality constant. In this work we maintain the energy density proportionality but set the parameter η so that the surface tension falls below 50 MeV fm^{-2}, a value consistent with those suggested for $\sigma(\chi)$ in recent literature [27–30].

3.2 Rare phase structure size, charge, and number density

The size of the rare phase structures is given by the radius (r) and is determined by minimizing the sum of the Coulomb and surface energies, $\frac{\partial(\epsilon_C+\epsilon_S)}{\partial r}$, and solving for r [3],

$$r = \left(\frac{D\sigma(\chi)}{4\pi e^2 f_D(\chi)\left[q_H(\chi) - q_Q(\chi)\right]^2}\right)^{\frac{1}{3}}. \quad (35)$$

The primitive cell of the lattice is taken to be the Wigner-Seitz cell, though it is simplified to have the same geometry as the rare phase structure. The Wigner-Seitz cell radius R is set so that the cell is charge neutral.

The density of electrons in the mixed phase is taken to be uniform throughout. Charge densities in both the rare and dominant phases are also taken to be uniform, an approximation supported by a recent study by Yasutake *et al.* [27]. The uniformity of charge in the rare phase also justifies the use of the nuclear form factor ($F(q)$) presented in sect. 4. The total charge number per unit volume ($|Z|/V_{\rm Rare}$) of the rare phase structures is given in fig. 2.

The number density of rare phase blobs will be important for calculating the phonon contribution to the emissivity. Since there is one rare phase blob per Wigner-Seitz cell, the number density of rare phase blobs (n_b) is simply the reciprocal of the Wigner-Seitz cell volume,

$$n_b = (4\pi R^3/3)^{-1}. \quad (36)$$

4 Neutrino emissivity in the quark-hadron mixed phase

Modeling the complex interactions of electrons with a background of neutrons, protons, hyperons, muons, and quarks is an exceptionally complicated problem. However, to make a determination of the neutrino emissivity that is due to electron-lattice interactions in the quark-hadron mixed phase we need only consider the Coulomb interaction between them. This simplifies the problem greatly, as a significant body of work exists for the analogous process of electron-ion scattering that takes place in the crusts of neutron stars.

4.1 Electron-lattice interaction

To determine the state of the lattice in the quark-hadron mixed phase we use the dimensionless ion coupling parameter given by [1]

$$\Gamma = \frac{Z^2 e^2}{R k_b T}\,. \tag{37}$$

Below $\Gamma_{\rm melt} = 175$ the lattice behaves as a Coulomb liquid, and above as a Coulomb crystal [1]. It was shown in Na *et al.* [12] that the emissivity due to electron-blob interactions in the mixed phase was insignificant compared to other contributions at temperatures above $T \gtrsim 10^{10}\,\mathrm{K}$. Therefore, in this work we consider temperatures in the range $10^7\,\mathrm{K} \leq T \leq 10^{10}\,\mathrm{K}$. At these temperatures the value of the ion coupling parameter is generally well above $\Gamma_{\rm melt}$, and so the lattice in the quark-hadron mixed phase is taken to be a Coulomb crystal.

To account for the fact that the elasticity of scattering events is temperature dependent we need to compute the Debye-Waller factor, which is known for spherical blobs only and requires the plasma frequency and temperature given by

$$\omega_p = \sqrt{\frac{4\pi Z^2 e^2 n_b}{m_b}}\,, \tag{38}$$

$$T_p = \frac{\hbar\omega_p}{k_b}\,, \tag{39}$$

where m_b is the mass of a spherical blob [11]. The Debye-Waller factor is then given by

$$W(q) = \begin{cases} \dfrac{\alpha q^2}{8k_e^2}\left(1.399e^{-9.1t_p} + 12.972t_p\right) & \text{spherical blobs,} \\ 0 & \text{rods and slabs,} \end{cases} \tag{40}$$

where $q = |\boldsymbol{q}|$ is a phonon or scattering wave vector, $\alpha = 4\hbar^2 k_e^2/(k_B T_p m_b)$, and $t_p = T/T_p$ [11,31]. In order to smooth out the charge distribution over the radial extent of the rare phase structure we adopt the nuclear form factor given in [11],

$$F(q) = \frac{3}{(qR^3)}\left[\sin(qR) - qR\cos(qR)\right]. \tag{41}$$

Screening of the Coulomb potential by electrons is taken into account by the static dielectric factor $\epsilon(q,0) = \epsilon(q)$, given in ref. [32]. However, the charge number of the rare phase structures is high and the electron number density is low, so setting this factor to unity has no noticeable effect on the calculated neutrino emissivity. Finally, the effective interaction is given by [11]

$$V(q) = \frac{4\pi e \rho_Z F(q)}{q^2 \epsilon(q)} e^{-W(q)}. \tag{42}$$

4.2 Neutrino emissivity

General expressions for the neutrino emissivity due to electron-lattice interactions were derived by Haensel *et al.* [33] for spherical blobs and by Pethick *et al.* [10] for rods and slabs,

$$Q_{\rm blobs} \approx 3.35 \times 10^{-67} n_b T^6 Z^2 L\ \mathrm{MeV\,s^{-1}\,fm^{-3}}, \tag{43}$$

$$Q_{\rm rods,slabs} \approx 3.00 \times 10^{-88}\, k_e T^8 J\ \mathrm{MeV\,s^{-1}\,fm^{-3}}, \tag{44}$$

where L and J are dimensionless quantities that scale the emissivities. Both L and J contain a contribution due to the static lattice (Bragg scattering), but we consider the additional contribution from lattice vibrations (phonons) for spherical blobs, so $L = L_{\rm sl} + L_{\rm ph}$.

4.3 Phonon contribution to neutrino emissivity

The expressions for determining the neutrino emissivity due to interactions between electrons and lattice vibrations (phonons) in a Coulomb crystal, with proper treatment of multi-phonon processes, were obtained by Baiko *et al.* [34] and simplified by Kaminker *et al.* [11]. The phonon contribution to the emissivity is primarily due to Umklapp processes in which a phonon is created (or absorbed) by an electron that is simultaneously Bragg reflected, resulting in a scattering vector $\boldsymbol{q}$ that lies outside the first Brillouin zone, $q_0 \gtrsim (6\pi^2 n_b)^{1/3}$ [35,36], where n_b is given by eq. (36).

The contribution to the neutrino emissivity due to phonons is contained in L_{ph} and given by eq. (21) in ref. [11],

$$L_{\rm ph} = \int_{y_0}^{1} \mathrm{d}y \frac{S_{\rm eff}(q)|F(q)|^2}{y|\epsilon(q,0)|^2}\left(1 + \frac{2y^2}{1-y^2}\ln y\right), \tag{45}$$

where $y = q/(2k_e)$, and the lower integration limit y_0 excludes momentum transfers inside the first Brillouin zone. The structure factor $S_{\rm eff}$ is given by eqs. (24) and (25) in ref. [11],

$$S_{\rm eff}(q) = 189\left(\frac{2}{\pi}\right)^5 e^{-2W} \int_0^\infty \mathrm{d}\xi \frac{1 - 40\xi^2 + 80\xi^4}{\left(1+4\xi^2\right)^5 \cosh^2(\pi\xi)} \times \left(e^{\Phi(\xi)} - 1\right), \tag{46}$$

$$\Phi(\xi) = \frac{\hbar q^2}{2m_b}\left\langle \frac{\cos(\omega_s t)}{\omega_s \sinh\left(\hbar\omega_s/2k_B T\right)} \right\rangle, \tag{47}$$

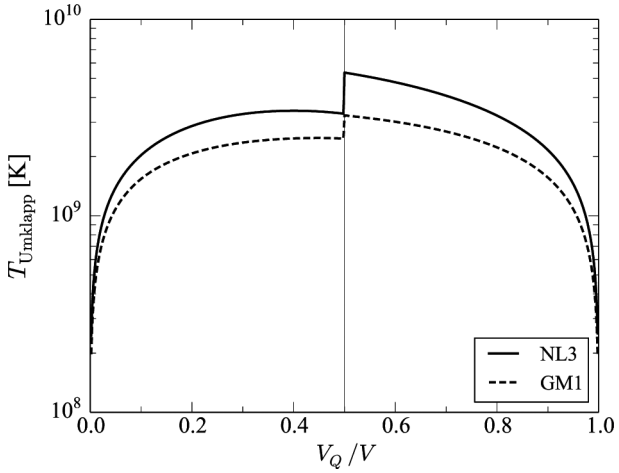

Fig. 3. Temperature below which Umklapp processes are frozen out ($T_{\rm Umklapp}$) as a function of quark fraction, and contributions to the neutrino emissivity due to electron-phonon interactions become negligible.

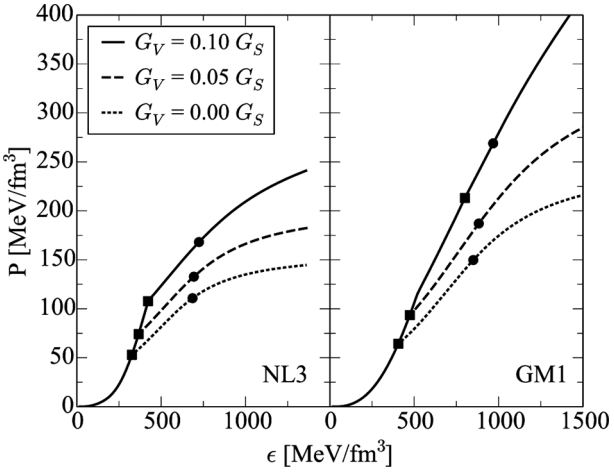

Fig. 4. Equations of state of this work. Shown are the hadronic and mixed phases. Square markers indicate the beginning of the quark-hadron mixed phase, and dot markers indicate the location of the maximum mass.

where $\xi = tk_BT/\hbar$ and $\langle\ldots\rangle$ denotes averaging over phonon frequencies and modes,

$$\langle f_s(\boldsymbol{k})\rangle = \frac{1}{3V_B}\sum_s \int_{V_B} \mathrm{d}\boldsymbol{k} f_s(\boldsymbol{k}). \tag{48}$$

It is assumed that there are three phonon modes s, two linear transverse and one longitudinal. The frequencies of the transverse modes are given by $\omega_{t_i} = a_i k$, where $i = 1, 2$, $a_1 = 0.58273$, and $a_2 = 0.32296$. The frequency of the longitudinal mode ω_l is determined by Kohn's sum rule, $\omega_l^2 = \omega_p^2 - \omega_{t_1}^2 - \omega_{t_2}^2$ [37].

Umklapp processes proceed as long as the temperature $T_{\rm Umklapp} \gtrsim T_p Z^{1/3} e^2/(\hbar c)$, below which electrons can no longer be treated in the free electron approximation [36]. This limits the phonon contribution to the neutrino emissivity to only a very small range in temperature for a crystalline quark-hadron mixed phase (see fig. 3), and renders it negligible compared to the static lattice contribution as will be shown in the next section.

4.4 Static lattice contribution to neutrino emissivity

Pethick and Thorsson [10] found that with proper handling of electron band-structure effects the static lattice contribution to the neutrino emissivity in a Coulomb crystal was significantly reduced compared to calculations performed in the free electron approximation. Kaminker *et al.* [11] presented simplified expressions for calculating the static lattice contribution ($L_{\rm sl}$) using the formalism developed in ref. [10]. The dimensionless quantities $L_{\rm sl}$ and J that scale the neutrino emissivities for spherical blobs and rods/slabs, respectively, are given by

$$L_{\rm sl} = \frac{1}{12Z}\sum_{K\neq 0}\frac{(1-y_K^2)}{y_K^2}\frac{|F(K)|^2}{|\epsilon(K)|^2} I(y_K, t_V) e^{-2W(K)} \tag{49}$$

and

$$J = \sum_{K\neq 0}\frac{y_K^2}{t_V^2} I(y_K, t_V), \tag{50}$$

where $K = |\boldsymbol{K}|$ is a scattering vector and restricted to linear combinations of reciprocal lattice vectors, $y_K = K/(2k_e)$, $t_V = k_BT/[|V(K)|(1-y_K^2)]$, and $I(y_K, t_V)$ is given by eq. (39) in ref. [11]. The sum over K in eqs. (49) and (50) terminates when $K > 2k_e$, prohibiting scattering vectors that lie outside the electron Fermi surface.

5 Results

The neutron star equation of state has been calculated using the relativistic mean-field approximation to describe the hadronic phase and the three-flavor nonlocal Nambu–Jona-Lasinio model for the quark phase, with the Gibbs condition governing the combination of the two in the mixed phase (fig. 4). Using the equation of state we solve the Tolman-Oppenheimer-Volkoff equation [38, 39] and find the mass-radius relationships given in fig. 5. The maximum masses of the neutron stars obtained for the given parameter sets are able to account for the recently discovered high-mass pulsars PSR J3048+0432 and PSR J1614-2230 [40–42], excluding GM1 with no vector coupling. It is evident from fig. 5 that increasing the vector coupling constant increases the maximum mass for the particular parameterization.

Figures 6 and 7 show the relative particle densities for the NL3 and GM1 parameterizations and three different values of the quark vector coupling constant. Hyperonization does not occur at all in the NL3 parameterization, as it is preceded by the low density onset of the quark-hadron phase transition at 2–3 times nuclear density. The same is true of the GM1 parameterization except in the case that $G_V = 0.10\,G_S$. Here the onset of the quark-hadron phase transition occurs at a much higher density

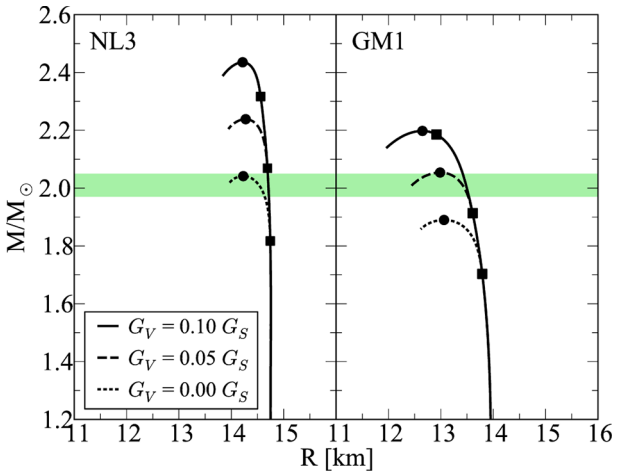

Fig. 5. (Color online) Mass-radius relationship of neutron stars for the given parameterizations and vector coupling constant values listed in table 1. Square markers indicate the beginning of the quark-hadron mixed phase, and dot markers indicate the location of the maximum mass. The green shaded region indicates the mass constraint set by PSR J3048+0432.

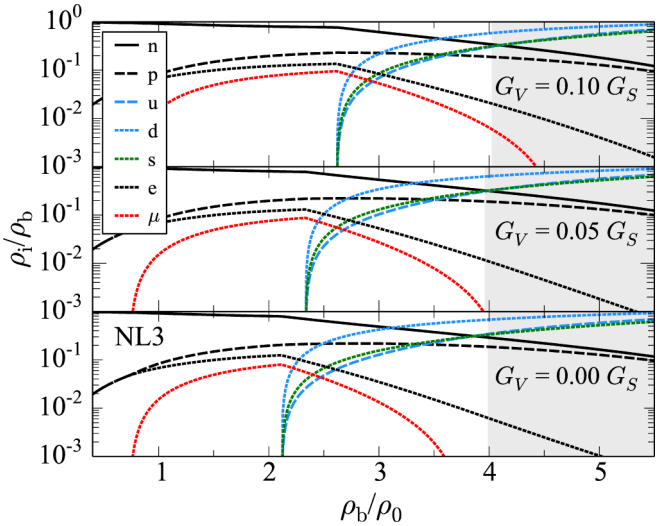

Fig. 6. (Color online) Relative particle number densities as a function of baryonic density (in units of nuclear saturation density) for the NL3 parameterization and given values of the vector coupling constant. Grey shaded region indicates densities beyond the maximum mass neutron star for the given parameterization.

due to the presence of the Ξ^- and Λ hyperons which soften the equation of state considerably, an effect that can be seen in the right panel of fig. 4. The low density onset of the quark-hadron phase transition is due in part to the choice of meson-hyperon coupling constants, which have been shown to postpone the onset of hyperonization, stiffening the low density equation of state [24]. Figure 5 shows that neutron stars within about 0.1–0.2 $M_\odot$ of their maximum mass contain a quark-hadron mixed phase in their core, with most possessing a maximum quark fraction of around 30% (see table 2).

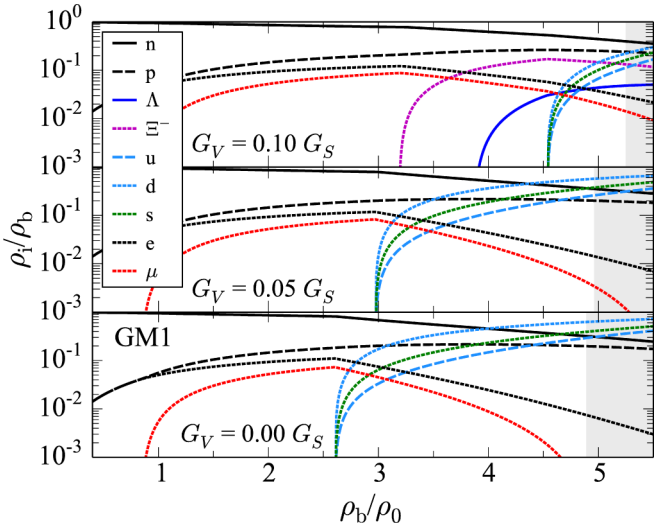

Fig. 7. (Color online) Same as fig. 6 but for the GM1 parameterization.

Table 2. Properties of the maximum mass neutron star for the given parameterizations.

	GM1			NL3		
G_V/G_S	0	0.05	0.10	0	0.05	0.10
$M/M_\odot$	1.89	2.05	2.20	2.04	2.24	2.43
$\chi_{\max}$	0.32	0.31	0.15	0.31	0.30	0.32
ρ_b [1/fm^3]	0.75	0.76	0.80	0.61	0.61	0.62
ϵ [MeV/fm^3]	851	883	969	687	696	726

Figure 8 shows the neutrino emissivity that is due to the crystalline structure of the quark-hadron mixed phase for all parameterizations and temperatures between 10^7–10^{10} K, as well as the modified Urca and bremsstrahlung (NN+QQ) emissivities for comparison. Electron-phonon interactions contribute to the neutrino emissivity when the mixed phase consists of spherical blobs ($\chi < 0.21$ and $\chi > 0.79$) and only at $T > T_{\rm Umklapp}$ (fig. 3). Figure 10 shows that the static-lattice contribution to the emissivity dominates the phonon contribution rendering it negligible, particularly at quark fractions relevant to the neutron stars of this work ($\chi \lesssim 0.3$). Equations (49) and (50) indicate that the static-lattice contribution is calculated as a sum over scattering vectors $N_{\boldsymbol{K}}$ that satisfy $K < 2k_e$. At the onset of the mixed phase the electron Fermi momentum k_e is at a maximum, which is particularly large in magnitude due to the lack of hyperons that would typically aid in the charge neutralization process. However, as the quark-hadron phase transition proceeds the negatively charged down and strange quarks take over the process of charge neutralization, resulting in a rapidly decreasing electron number density ($k_e = (3\pi^2 n_e)^{\frac{1}{3}}$). This and the exponentially decreasing size of the Wigner Seitz cell in the spherical blob phase ($\chi < 0.21$) lead to the steep decline in $N_{\boldsymbol{K}}$ (fig. 11), which accounts for the rapid decrease of the neutrino emissivity in the mixed phase.

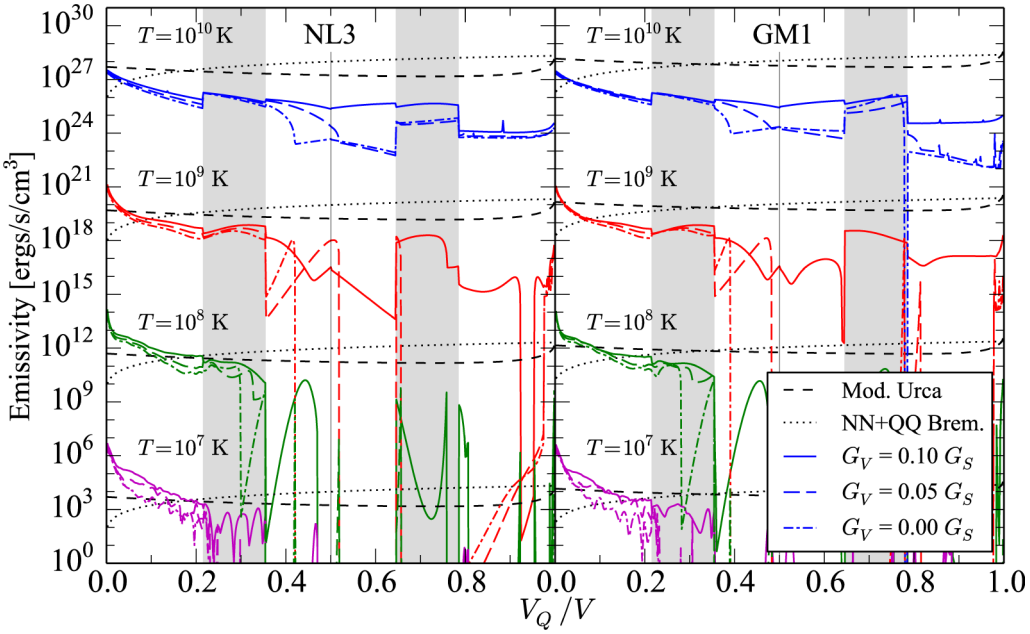

Fig. 8. (Color online) Comparison of the neutrino emissivity due to electron-lattice interactions in the quark-hadron mixed phase to modified Urca and bremsstrahlung (NN+QQ) processes in the mixed phase for different parameterizations [43]. Shading represents geometric structures as shown in fig. 9.

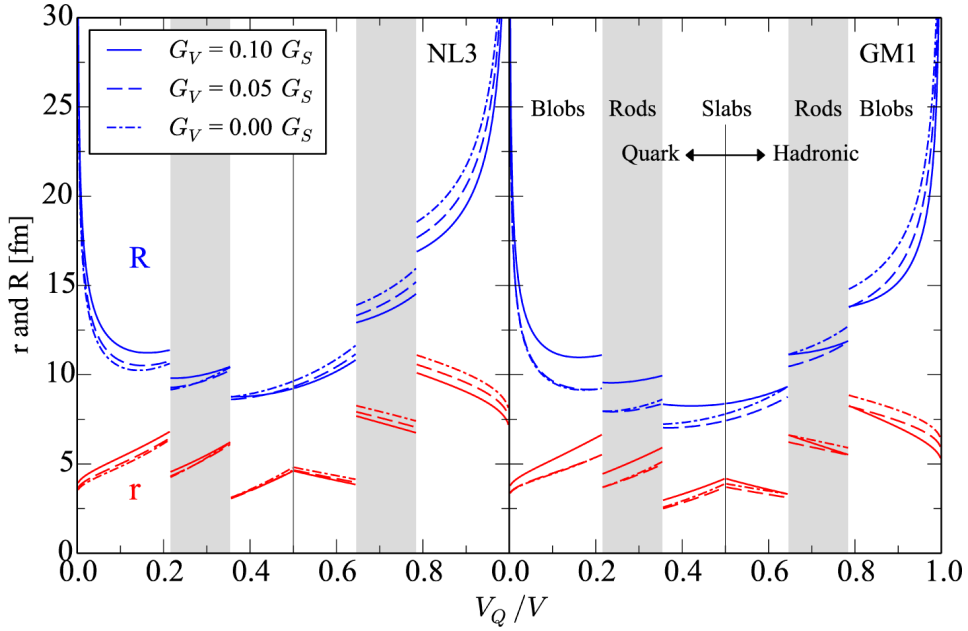

Fig. 9. (Color online) Rare phase structure radius r and Wigner-Seitz cell radius R plotted against quark fraction for the given parameterizations and vector coupling constant values. The change in background color refers to a change in structure as shown in the right panel. Discontinuities in the radii are also associated with changes in the crystalline structure.

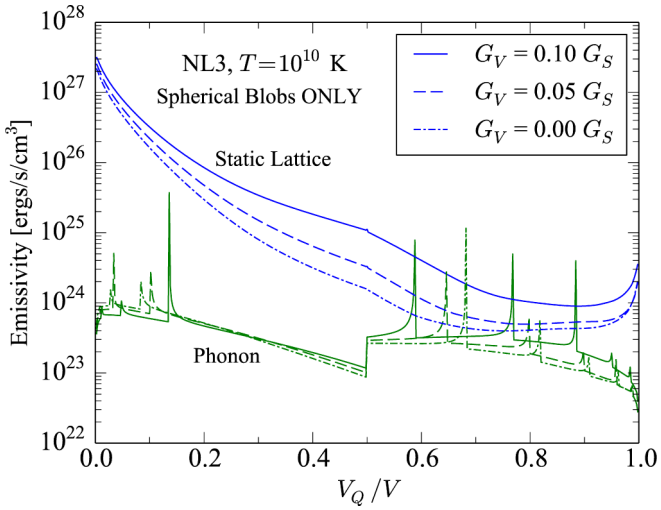

Fig. 10. (Color online) Comparison of the static lattice and phonon contributions to the neutrino emissivity for the NL3 parameter set at $T > T_{\rm Umklapp}$. The comparison is performed for only the spherical blob geometry, as the phonon contribution is not determined for other geometries.

The geometrical structure of the quark-hadron mixed phase terminates with the rod phase at $\chi \sim 0.3$ for nearly all the chosen parameterizations. Up to this point the neutrino emissivity due to the structure of the mixed phase is either larger or comparable to the modified Urca and bremsstrahlung (NN+QQ) emissivities for $T \lesssim 10^8$ K. The emissivities in the NL3 and GM1 parameterizations are comparable, though the effect of the mixed phase structure appears more substantial for NL3 due to lower modified Urca and bremsstrahlung (NN+QQ) emissivities. The emissivity at very low quark fraction ($\chi \lesssim 0.05$) may be overestimated due to the finite blob radius at $\chi = 0$ that results from the fact that $f_d(0) = 0.4$. Finally, beyond the rod-slab structure transition at $\chi \approx 0.35$ the electron-lattice contribution to the overall neutrino emissivity is negligible, though this is beyond the extent of the mixed phase of the neutron stars in this work.

6 Summary and conclusions

Exploring the properties of compressed baryonic matter, or, more generally, strongly interacting matter at high densities and/or temperatures, has become a forefront area of modern physics [44]. Experimentally, such matter is being created in relativistic particle colliders such as the Relativistic Heavy Ion Collider RHIC at Brookhaven and the Large Hadron Collider (LHC) at Cern, and great advances in our understanding of such matter are expected from the next generation of collision experiments at FAIR (Facility for Antiproton and Ion Research at GSI) and NICA (Nucloton-based Ion Collider fAcility at JINR) [45, 46].

Complementary to these experiments, astrophysics provides a natural laboratory in which to explore the physics of compressed baryonic matter too (see [47–49] and references therein). The Hubble Space Telescope and X-ray satellites such as Chandra and XMM-Newton in particular have proven especially valuable. New astrophysical instruments such as the Five hundred meter Aperture Spherical Telescope (FAST), the square kilometer Array (skA), Fermi Gamma-ray Space Telescope (formerly GLAST), Astrosat, ATHENA (Advanced Telescope for High ENergy Astrophysics), and the Neutron Star Interior Composition Explorer (NICER) promise the discovery of tens of thousands of new neutron stars. Of particular interest will be the proposed NICER mission, which is dedicated to the study of the extraordinary gravitational, electromagnetic, and nuclear-physics environments embodied by neutron stars. NICER will explore the exotic states of matter in the core regions of neutron stars, confronting nuclear theory with unique observational constraints.

With that in mind, we focus in this paper on quark deconfinement in the cores of neutron stars. The neutron star equation of state for cold catalyzed matter ($T \lesssim 1$ MeV) has been determined using the relativistic mean-field (RMF) approximation to model the hadronic phase and the nonlocal three-flavor Nambu-Jona-Lasinio model (n3NJL) for the quark phase. The mass-radius results indicate that a neutron star containing quark matter in the core can account for the high mass of the recently discovered pulsars PSR J3048+0432 and PSR J1614-2230, and that a maximum mass neutron star can be expected to contain approximately 30% quark matter at the center. If the surface tension between hadronic and quark matter is low as suggested in the recent literature, a phase transition that results in a mixed phase will occur in the core of a neutron star. The relaxed condition of global charge neutrality will lead to charge segregation in the mixed phase resulting in the formation of a crystalline lattice of quark matter immersed in a hadronic matter background. Expanding on Na *et al.* [12], we considered the presence of two additional geometrical structures in the mixed phase in addition to spherical blobs: rods, and slabs (fig. 1).

Using the formalism developed for analogous neutrino-pair bremsstrahlung processes in the neutron star crust we have estimated the neutrino emissivity due to electron-lattice interactions in the quark-hadron mixed phase. The emissivity is highly dependent on the electron number density, which has been shown to decrease considerably in the presence of negatively charged hyperons and quarks (figs. 6 and 7). However, we have shown that at temperatures between 10^7 K and 10^9 K and quark fractions less than around 30% the neutrino emissivity due to electron-lattice interactions is significant when compared to the standard baryon and quark modified Urca and bremsstrahlung (NN+QQ) processes (fig. 8). Further, we have also shown that the emissivity due to electron-phonon interactions is insignificant compared to contributions from Bragg diffraction at temperatures above which Umklapp processes are frozen out (fig. 10).

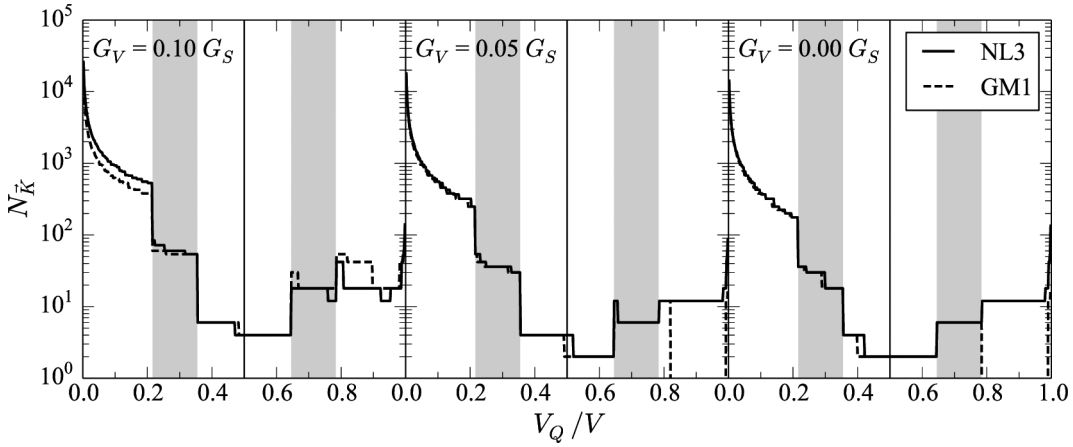

Fig. 11. (Color online) The number of scattering vectors that satisfy the condition $K < 2k_e$ as a function of the quark fraction in the mixed phase for the equations of state of this work.

Before we can determine the effect the presence of quark matter and the crystalline structure of the quark-hadron mixed phase has on the thermal evolution of a neutron star the following steps need to be taken. First, RMF should be replaced with a model for hadronic matter that softens the equation of state and produces results for neutron star radii that are more compatible with observations and recent statistical studies (see, for example, [50, 51]). To this end, we are currently working on combining an RMF model that accounts for density dependence in the values of the meson-baryon coupling constants with the three-flavor n3NJL model (see, for example, [52–59]). Next, the thermal conductivity and specific heat should be calculated for the quark-hadron mixed phase as outlined in Na *et al.* [12] using the updated equation of state for quark matter (n3NJL) and accounting for additional rare phase geometries (rods, slabs). Finally, these results would be incorporated into a neutron star cooling simulation capable of properly accounting for the complexity of the crystalline quark-hadron mixed phase.

This work is supported through the National Science Foundation under grants PHY-1411708 and DUE-1259951. Additional computing resources are provided by the Computational Science Research Center and the Department of Physics at San Diego State University. GAC and MGO acknowledge financial support by CONICET and UNLP (Project identification code 11/G119), Argentina.

References

1. P. Haensel, A.Y. Potekhin, D.G. Yakovlev, *NEUTRON STARS 1: Equation of State and Structure* (Springer, New York, 2007).
2. F. Weber, Prog. Part. Nucl. Phys. **54**, 193 (2005).
3. N.K. Glendenning, Phys. Rep. **342**, 393 (2001).
4. N.K. Glendenning, Phys. Rev. D **46**, 1274 (1992).
5. E. Flowers, Astrophys. J. **180**, 911 (1973).
6. N. Itoh, Y. Kohyama, Astrophys. J. **275**, 858 (1984).
7. N. Itoh, N. Matsumoto, M. Seki, Y. Kohyama, Astrophys. J. **279**, 413 (1984).
8. N. Itoh, Y. Kohyama, N. Matsumoto, M. Seki, Astrophys. J. **280**, 787 (1984).
9. N. Itoh, Y. Kohyama, N. Matsumoto, M. Seki, Astrophys. J. **285**, 304 (1984).
10. C.J. Pethick, V. Thorsson, Phys. Rev. D **56**, 7548 (1997).
11. A.D. Kaminker, C.J. Pethick, A.Y. Potekhin, V. Thorsson, D.G. Yakovlev, Astron. Astrophys. **343**, 1009 (1999).
12. X. Na, R. Xu, F. Weber, R. Negreiros, Phys. Rev. D **86**, 123016 (2012).
13. F. Weber, *Pulsars as Astrophysical Laboratories for Nuclear and Particle Physics*, in *Studies in High Energy Physics, Cosmology, and Gravitation* (IoP Publishing, Bristol, 1999).
14. G. Baym, C.J. Pethick, P. Sutherland, Astrophys. J. **170**, 299 (1971).
15. G. Baym, H.A. Bethe, C.J. Pethick, Nucl. Phys. A **175**, 225 (1971).
16. J.D. Walecka, Ann. Phys. (N.Y.) **83**, 491 (1974).
17. N.K. Glendenning, Astrophys. J. **293**, 470 (1985).
18. N.K. Glendenning, *Compact Stars: Nuclear Physics, Particle Physics, and General Relativity*, 2nd edition (Springer-Verlag, New York, 2000).
19. J. Boguta, A.R. Bodmer, Nucl. Phys. A **292**, 413 (1977).
20. J. Boguta, J. Rafelski, Phys. Lett. B **71**, 22 (1977).
21. J. Boguta, H. Stöcker, Phys. Lett. B **120**, 289 (1983).
22. M. Orsaria, H. Rodrigues, F. Weber, G.A. Contrera, Phys. Rev. D **87**, 023001 (2013).
23. M. Orsaria, H. Rodrigues, F. Weber, G.A. Contrera, Phys. Rev. C **89**, 015806 (2014).
24. T. Miyatsu, M. Cheoun, K. Saito, Phys. Rev. C **88**, 015802 (2013).
25. T.A. Rijken, M.M. Nagels, Y. Yamamoto, Prog. Theor. Phys. Suppl. **185**, 14 (2010).
26. P. Rehberg, S.P. Klevansky, J. Hufner, Phys. Rev. C **53**, 410 (1996).
27. N. Yasutake, R. Lastowiecki, S. Benic, D. Blaschke, T. Maruyama, T. Tatsumi, Phys. Rev. C **89**, 065803 (2014).
28. L.F. Palhares, E.S. Fraga, Phys. Rev. D **82**, 125018 (2010).
29. M.B. Pinto, V. Koch, J. Randrup, Phys. Rev. C **86**, 025203 (2012).
30. B.W. Mintz, R. Stiele, R.O. Ramos, J. Schaffner-Bielich, Phys. Rev. D **87**, 036004 (2013).
31. D.A. Baiko, D.G. Yakovlev, Astron. Lett. **21**, 702 (1995).

32. N. Itoh, Y. Kohyama, Astrophys. J. **275**, 858 (1983).
33. P. Haensel, A.D. Kaminker, D.G. Yakovlev, Astron. Astrophys. **314**, 328 (1996).
34. D.A. Baiko, A.D. Kaminker, A.Y. Potekhin, D.G. Yakovlev, Phys. Rev. Lett. **81**, 5556 (1998).
35. J.M Ziman, *Principles of the Theory of Solids* (Cambridge University Press, Cambridge, 1972).
36. M.E. Raikh, D.G. Yakovlev, Astrophys. Space Sci. **87**, 193 (1982).
37. R. Mochkovitch, J.P. Hansen, Phys. Lett. A **73**, 35 (1979).
38. R.C. Tolman, Phys. Rev. **55**, 364 (1939).
39. J.R. Oppenheimer, G.M. Volkoff, Phys. Rev. **55**, 374 (1939).
40. P.B. Demorest, T. Pennucci, S.M. Ranson, M.S.E. Roberts, J.W.T. Hessels, Nature **467**, 1081 (2010).
41. R.S. Lynch *et al.*, Astrophys. J. **763**, 81 (2013).
42. J. Antoniadis *et al.*, Science **340**, 6131 (2013).
43. N. Iwamoto, Ann. Phys. **141**, 1 (1982).
44. P. Braun-Munzinger, J. Wambach, Rev. Mod. Phys. **81**, 1031 (2009).
45. B. Friman, C. Höhne, J. Knoll, S. Leupold, R. Randrup, J. Rapp, P. Senger (Editors), *Lecture Notes in Physics*, Vol. **814** (Springer, 2011) p. 960.
46. See NICA White Paper at `http://nica.jinr.ru/files/WhitePaper.pdf`.
47. W. Becker (Editor), *Neutron Stars and Pulsars*, in *Astrophysics and Space Science Library*, Vol. **357** (Springer, 2009) p. 697.
48. J. van Leeuwen (Editor), *Neutron Stars and Pulsars: Challenges and Opportunities after 80 years*, IAU Symposium No. 291, (Cambridge University Press, 2013) p. 592.
49. M. Buballa *et al.*, J. Phys. G: Nucl. Part. Phys. **41**, 123001 (2014).
50. A.W. Steiner, J.M. Lattimer, E.F. Brown, Astrophys. J. **722**, 33 (2010).
51. J.M. Lattimer, Annu. Rev. Nucl. Part. Sci. **62**, 485 (2012).
52. C. Fuchs, H. Lenske, H.H. Wolter, Phys. Rev. C **52**, 3043 (1995).
53. S. Typel, H.H. Wolter, Nucl. Phys. A **656**, 331 (1999).
54. F. Hofmann, C.M. Keil, H. Lenske, Phys. Rev. C **64**, 025804 (2001).
55. C.-Y. Ryu, C.H. Hyun, C.-H. Lee, Phys. Rev. C **84**, 035809 (2011).
56. G. Colucci, A. Sedrakian, Phys. Rev. C **87**, 055806 (2013).
57. E.N.E. van Dalen, G. Colucci, A. Sedrakian, Phys. Lett. B **734**, 383 (2014).
58. M. Oertel, C. Providencia, F. Gulminelli, Ad.R. Raduta, J. Phys. G **42**, 075202 (2015).
59. S. Benic, D. Blaschke, D.E. Alvarez-Castillo, T. Fischer, S. Typel, Astron. Astrophys. **577**, A40 (2015).